I&EC research
Industrial & Engineering Chemistry Research

Article

pubs.acs.org/IECR

Surface Modification of Graphene with Layered Molybdenum Disulfide and Their Synergistic Reinforcement on Reducing Fire Hazards of Epoxy Resins

Dong Wang,[†] Keqing Zhou,[†] Wei Yang,[†] Weiyi Xing,[†] Yuan Hu,*[,†,‡] and Xinglong Gong*[,†,§]

[†]State Key Laboratory of Fire Science, University of Science and Technology of China, 96 Jinzhai Road, Hefei, Anhui 230026, People's Republic of China

[‡]USTC-CityU Joint Advanced Research Centre, Suzhou Key Laboratory of Urban Public Safety, Suzhou Institute for Advanced Study, University of Science and Technology of China, 166 Ren'ai Road Suzhou, Jiangsu 215123, People's Republic of China

[§]CAS Key Laboratory of Mechanical Behaviour and Design of Materials, Department of Modern Mechanics, University of Science and Technology of China, Hefei, Anhui 230026, People's Republic of China

ABSTRACT: In this work, molybdenum disulfide (MoS_2)−modified graphene (MoS_2/GNS) hybrids were prepared by the hydrothermal method and characterized by X-ray diffraction (XRD), Laser Raman spectroscopy (LRS) and transmission electron microscope (TEM). The characterization results show layered molybdenum disulfide was deposited on the surface of graphene nanosheets (GNSs) and grahene oxide was reduced simultaneously. Thermogravimetric analysis results of MoS_2, GNS and MoS_2/GNS hybrids showed that incorporation of MoS_2 increased the thermal oxidation resistance of the graphene evidently. Compared to pure epoxy resins (EP), the addition of MoS_2/GNS hybrids into EP enhanced the onset thermal degradation temperature (T_{onset}) with an 53 °C increment under air atmosphere and an 18 °C increment under nitrogen atmosphere. The addition of MoS_2/GNS hybrids endows excellent flame retardant properties to EP, confirmed by the dramatically reduced peak heat release rate value and total heat release value. Moreover, the addition of MoS_2/GNS hybrids dramatically decreased the smoke products.

1. INTRODUCTION

As a prospective category of layered material, graphene nanosheets (GNSs), have been broadly researched in numerous domains such as conductive materials,[1] energy devices,[2,3] sensors,[4] polymer nanocomposites,[5] because of the peculiar structure, superior electrical conductivity, excellent thermal and mechanical performances. In recent years, GNSs have given rise to continuous attention in fire safety.[6−10] Kim et al.[11] have demonstrated that graphene is actually thermal stability, even exposed to a fire, distinctly declaring that it has highly essential fire resistance. Nevertheless, high loading of bare graphene is required to achieve good flame retardant properties. Therefore, to improve flame retardant efficiency of bare graphene seems to be an appealing and challenging work. In our previous work, functionalizing graphene with polyhedral oligomeric silsesquioxan (OapPOSS)[12] and loading transition metal oxides,[13] layered double hydroxides (LDHs),[14] etc. on the surface of graphene are two valid way to improve flame retardant efficiency of graphene.

At the same time, the specific two dimension (2D) structure of graphene also has aroused much interest on 2D layered materials. As one of the most potential layered materials, molybdenum disulfide (MoS_2) has the homologous structure of GNS, which is comprised of three stacked atom layers (S−Mo−S) associated by van der Waals forces[15] and has attracted more and more attention from various fields such as transistors,[16] catalysts,[17] composites.[18] Over the past few years, researchers have begun to study the application of MoS_2 in fire safety. Zhou et al.[19] have confirmed that MoS_2 can improve flame retardant properties of poly(vinyl alcohol) (PVA). Furthermore, Matusinovic et al.[20] have shown the addition of 10 wt % MoS_2 into polystyrene and poly(methyl methacrylate) can lead to a significant reduction in their peak heat release rate (PHRR) as well.

Epoxy is a thermoset resin applied in numerous industries, such as coating, binder, and composite materials, due to its excellent mechanical and chemical properties. However, fire hazards exist in the application of EP, because of its inflammability. Due to the remarkable barrier effect of GNSs, GNSs could effectively inhibit the heat release and pyrolysis products during the combustion of epoxy.[21−24] Nevertheless, the oxidation of GNSs at high temperature would fade the barrier effect. Thus, it is a serious subject to improve thermal oxidative resistance of GNSs. Surface modification of GNSs with layered compounds is a valid way to inhibit oxygen from accessing GNSs. 2D layered MoS_2 is a good choice, and MoO_3 obtained by the oxidation of MoS_2 is a highly efficient smoke suppressant. Furthermore, there are few reports about the influence of MoS_2 on fire behavior of epoxy until now. So, it would be an interesting and meaningful work to investigate the influence of MoS_2 on fire behavior of epoxy.

In our present work, layered MoS_2/GNS hybrids were synthesized by the hydrothermal method and MoS_2/GNS/

Received: July 29, 2013
Revised: November 20, 2013
Accepted: November 28, 2013
Published: November 28, 2013

dx.doi.org/10.1021/ie402441g | *Ind. Eng. Chem. Res.* 2013, 52, 17882−17890

epoxy (MoS_2/GNS/EP) composites were prepared by a simple blend under ultrasonic agitation. Synergistic effect between MoS_2 and GNS on thermal stability and fire hazards was investigated by thermogravimetric analysis (TGA), micro-combustion calorimeter (MCC), and cone calorimeter. Moreover, the flame retardant mechanism was studied by the analysis of char residue after the cone calorimeter test.

2. EXPERIMENTAL SECTION

2.1. Materials. Graphite powder, $Na_2MnO_4{\cdot}2H_2O$, thiourea, concentrated sulfuric acid (98%), sodium nitrate, potassium permanganate, 30% H_2O_2 solution, hydrochloric acid, and 4,4′-diaminodiphenyl methane (DDM, AP) were all purchased from Sinopharm Chemical Reagent Co. Ltd. (Shanghai, China). Epoxy resin (E-44) with epoxy value about 0.44 mol/100 g was obtained from Hefei Jiangfeng chemical industry co., Ltd. (China). All chemicals were employed as they came without further treatment. Distilled water is used for the total experiment except as otherwise noted.

2.2. Synthesis of MoS_2/GNS Hybrids. Graphene oxide (GO) was prepared from graphite via the Hummers' method.[25] Layered MoS_2/GNS hybrids were synthesized via a tradition hydrothermal method, as shown in Scheme 1a. In a typical procedure, $Na_2MoO_4{\cdot}2H_2O$ (0.3 g) and thiourea (0.8 g) were dissolved in 400 mL of distilled water, and then 100 mg of the as-prepared GO was added into the solution. The blend was stirred under ultrasound to get a homogeneous solution. Subsequently, the above homogeneous solution was transferred into a 500 mL Teflon-lined autoclave and held at 200 °C for 24 h. After that, the autoclave was put to cool to indoor temperature, and the generated samples were separated by centrifugation, washed with distilled water and ethanol, and then dried at 80 °C for 12 h.

Scheme 1. Preparation Routes of (a) MoS_2/GNS Hybrids and (b) MoS_2/ GNS/EP Composites

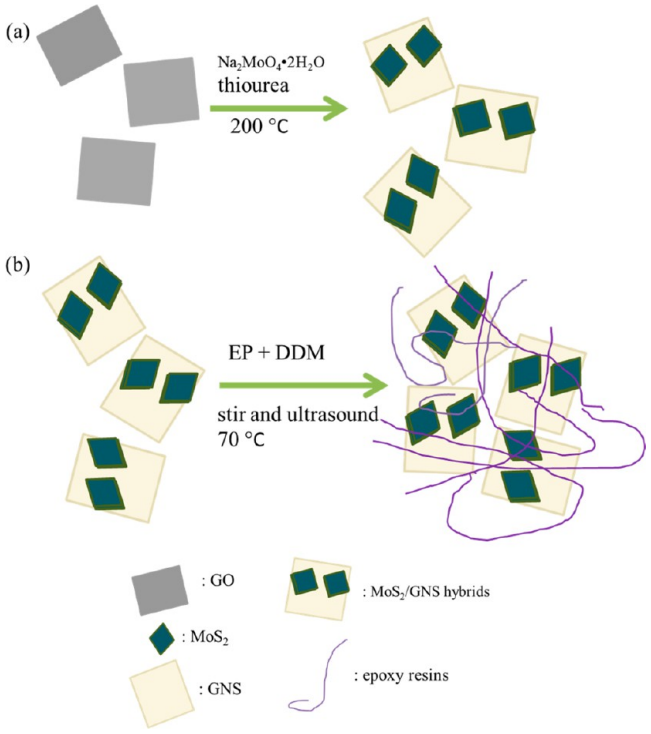

2.3. Preparation of MoS_2/GNS/epoxy (MoS_2/GNS/EP) Composites. MoS_2/ GNS/EP composites were prepared using a simple blend under ultrasonic agitation, as displayed in Scheme 1b. In brief, the preparation of epoxy composite with 2 wt % MoS_2/GNS hybrids was operated as follows: the blends of liquid epoxy resins (8.2 g) and MoS_2/GNS (0.2 g) were stirred and ultrasonicated at 70 °C. Then, powdered DDM (1.6 g) was added to the blend above and stirred till the intermixtures were obtained. Subsequently, the composites were cured at 100 °C for 2 h and post cured at 150 °C for 2 h. After curing, the composites were cooled to room temperature. Pure EP, MoS_2/EP, and GNS/EP composites were prepared via the same procedure.

2.4. Characterization. X-ray diffraction (XRD) measurements were implemented on a Japan Rigaku D Max-Ra rotating anode X-ray diffractometer equipped with a Cu-Kα tube and Ni filter (λ = 0.1542 nm). The scanning rate was 4°/min, and the range was 10−70°.

Laser Raman spectroscopy (LRS) measurements were carried out at room temperature with a SPEX-1403 laser Raman spectrometer (SPEX Co., U.S.A.) with excitation provided in backscattering geometry by a 514.5 nm argon laser line.

The morphology and structure of MoS_2/GNS were studied by transmission electron microscopy (TEM, JEM-2100F, Japan Electron Optics Laboratory Co., LTD, Japan) with an accelerating voltage of 200 kV. MoS_2/GNS hybrids were dispersed in deionized water with ultrasonication and then dripped onto copper grids before observation.

Thermal gravimetric analysis (TGA) of samples was carried out using a Q5000 IR (TA Instruments) thermal analyzer from room temperature to 700 °C at a heating rating of 20 °C/min.

A micro-combustion calorimeter (MCC, GOVMARK) was used to evaluate the combustion properties of the samples according to ASTM D 7309-07. Samples of 4−6 mg were heated in nitrogen atmosphere at a constant heating rate 1 °C/s from room temperature to 650 °C. The decomposition products were mixed with 20 mL/min oxygen and then burned in the combustion furnace at 900 °C.

Fire hazards, including PHRR (peak heat release rate), THR (total heat release), TSR (total smoke release), and SPR (smoke production rate), of samples were performed on a cone calorimeter (Fire Testing Technology, U.K.) according to ASTM E1354/ISO 5660. Each sample (100 × 100 × 3 mm^3) was wrapped in an aluminum foil and exposed horizontally to a 35 kW/m^2 external heat flux.

Scanning electron microscopy (SEM) pictures of the samples were taken employing a DXS-10 scanning electron microscope (Shanghai Electron Optical Technology Institute). The sample was placed on the copper plate and then coated with gold/palladium alloy ready for imaging.

3. RESULT AND DISCUSSION

3.1. Characterization of MoS_2/GNS Hybrids. The XRD patterns of the as-prepared pure MoS_2 and MoS_2/GNS hybrids are displayed in Figure 1. Pure MoS_2 exhibits the typical profile of the standard MoS_2 nanocrystal with a hexagonal structure. The characteristics bands at 2θ = 14.1°, 33.3°, 39.8°, 49.7°, and 59.2° are assigned to the (002), (100), (103), (105), and (110) diffraction peaks, respectively. The characteristic bands of MoS_2/GNS hybrids are similar to that of pristine MoS_2, except a very weak band at 2θ = 26.0°. The very weak band belongs to the (002) diffraction peak of GNS, due to the introduction of

dx.doi.org/10.1021/ie402441g | Ind. Eng. Chem. Res. 2013, 52, 17882−17890

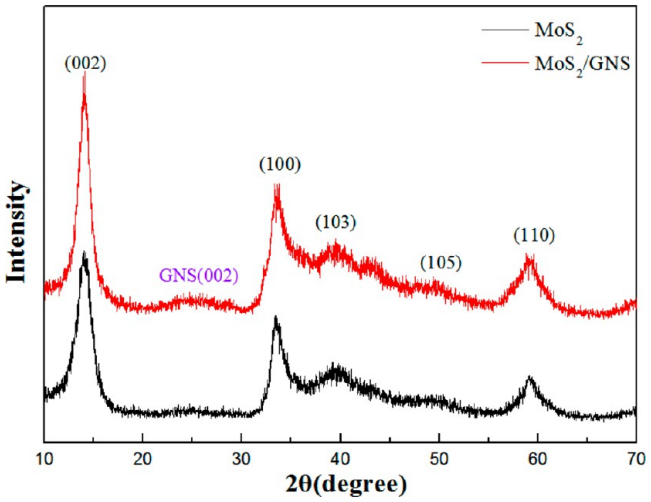

Figure 1. Typical XRD patterns of the prepared MoS_2 and MoS_2/GNS hybrids.

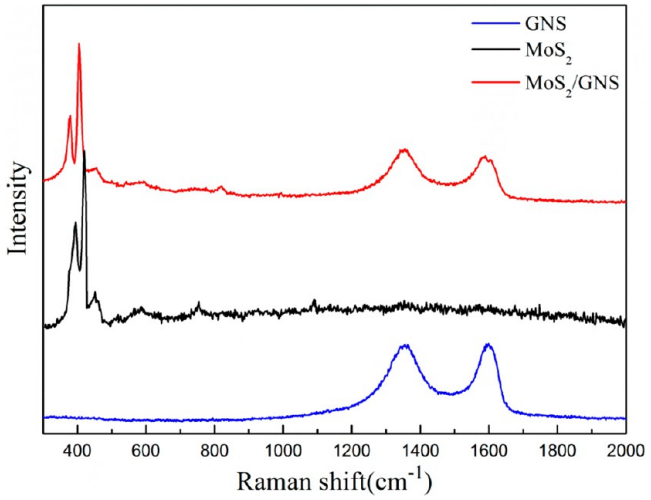

Figure 2. Raman spectrum of the prepared MoS_2, GNS, and MoS_2/GNS hybrids.

MoS_2 on the surface of GNS.[22] Besides, no excess peaks have been shown, so ensuring the lack of contaminant phases.

Figure 2 shows the Raman spectrum of the as-prepared MoS_2, GNS and MoS2/GNS hybrids. Two obvious Raman featured peaks at 406 and 383 cm^{-1} for the MoS_2 nanosheets can be observed, which arise from the A_{1g} and E_{2g} modes, respectively.[26] Furthermore, the peaks about 1370 and 1600 cm^{-1} are in charge of the D and G bands of the GNS, respectively. The G band is mainly associated with the in-plane bond stretching of pairs of sp^2 C atoms, while the D mode is attributed to defects or lattice distortion.[27]

The morphology and microstructure of MoS_2/GNS hybrids are displayed in Figure 3. As can be observed from Figure 3a, GNS reveals a typically flat nanosheet shape which is a few hundred nanometers size. Parts b and c of Figure 3 show TEM images of the hybrids, which show a classical wrinkled and ripped morphology. The high-resolution TEM image (Figure 3d) reveals that layered MoS_2 nanosheets of a few layers with an interlayer distance of 0.62 nm are covered on the surface of the GNS, suggesting that the MoS_2/GNS hybrids have been successfully synthesized and a few layered GNS with few layers and an interlayer distance of 0.34 nm exist, consistent with the existence of a very weak diffraction peak ($\sim 2\theta$ = 26.0°) of GNS.

The effect of MoS_2 on the thermal oxidative resistance of graphene was studied by thermogravimetric analysis (TGA). Figure 4 shows TGA results of GNS, MoS_2 and MoS_2/GNS hybrids performed under air at a heating rate of 20 °C·min^{-1}. Pristine GNS displays a continuous mass loss, which could be ascribed to the volatilization of adsorbed water and then the oxidation of graphene. MoS_2 shows a three-stage thermogravimetric curves corresponding to the evaporation of physisorbed water (from room temperature to 300 °C), the loss of chemisorbed water (300−400 °C), and the oxidation of MoS_2 to molybdenum oxide and sulfur dioxide (400−450 °C), respectively. In contrast, the resultant MoS_2/GNS hybrids demonstrate a similar thermogravimetric curve to pure GNS. The earlier temperature of the maximum mass loss rate is attributed to the oxidation of MoS_2 on the surface of GNS and the residue percentage of MoS_2/GNS hybrids do not change hardly from 500 °C, suggesting MoS_2 inhibits oxidation of underlying GNS. Moreover, the residual percentage of the MoS_2/GNS hybrids is much higher than that of graphene, suggesting that the modification of MoS_2 on the surface of GNS obviously enhances the thermal oxidative resistance of graphene.

3.2. Thermal Degradation of Composites. Thermogravimetric analysis is an important method to estimate thermal behavior for polymer materials. Because air content of combustion surface is different from that of combustion interior, thermal degradation of surface materials differs from that of internal materials. TG and DTG cures under nitrogen (N_2) atmosphere display thermal degradation of pure EP and its composites interior during combustion, whereas TG and DTG profiles under air atmosphere show thermal degradation of pure EP and its composites surface during combustion, as can be observed in Figure 5.

3.2.1. Thermal Degradation under N_2 Atmosphere. Parts a and c of Figure 5 show TG/DTG profiles for EP and its composites as a function of temperature under N_2 atmosphere. The definition of the onset degradation temperature (T_{onset}) and the maximum degradation temperature(T_{max}) are the temperature at which the mass loss are 5% and maximum, respectively. The oxidation of GNS or MoS_2 would not occur under N_2 atmosphere, indicating that barrier effect of GNS or MoS_2 would play the most important role on thermal degradation of composites. After incorporating GNS or MoS_2 into epoxy, their T_{onset} show a slight increase compared with pure EP, ascribed to that the barrier effect of layered GNS or MoS_2 inhibit the release of the decomposition products. When graphene is modified with MoS_2, the MoS_2/GNS/EP composites have the best thermal stability on T_{onset} with an 18 °C increment. Furthermore, char yields for GNS/EP and MoS_2/EP composites are higher than that for pure EP, demonstrating that the barrier effect of GNS and MoS_2 to inhibit the mass loss would promote catalytic carbonization of epoxy. Additionally, DTG curves show that the maximum mass loss rate of the MoS_2/GNS/EP composites is the lowest, suggesting that MoS_2 and GNS have a synergistic effect on the physical barrier to prevent the weight loss of the matrix.

3.2.2. Thermal Degradation under Air Atmosphere. As can be observed in Figure 5d, the thermal degradation process of pristine epoxy and its composites have three steps, which are the volatilization of absorbed water, the decomposition of the macromolecular chains, and the oxidation of the residual char.

dx.doi.org/10.1021/ie402441g | Ind. Eng. Chem. Res. 2013, 52, 17882−17890

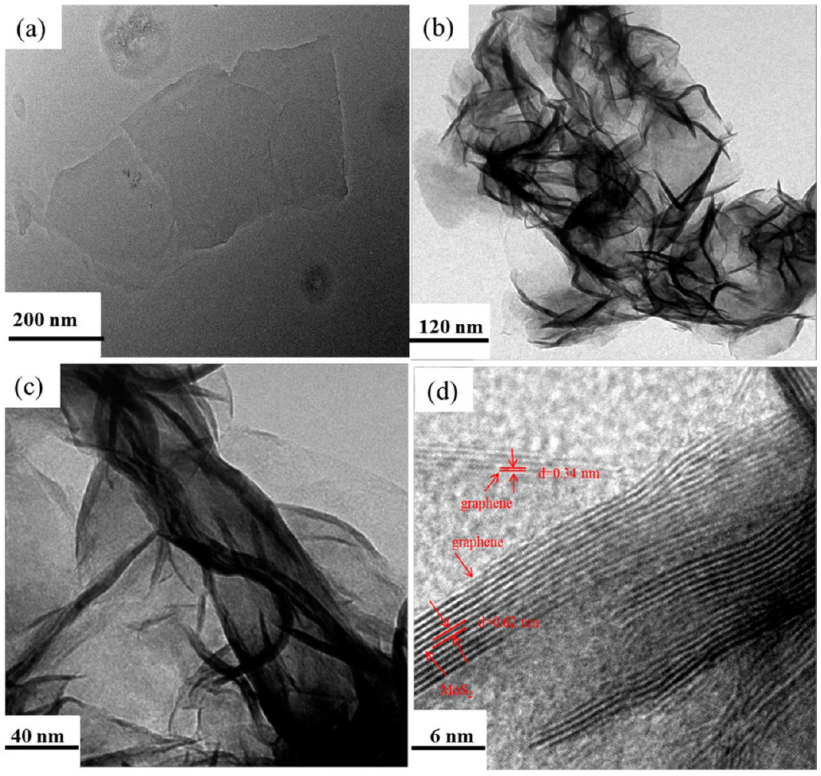

Figure 3. TEM image of (a) GNS; (b and c) layered MoS_2/GNS hybrids at different magnifications; (d) high-resolution TEM image of layered MoS_2/GNS hybrids.

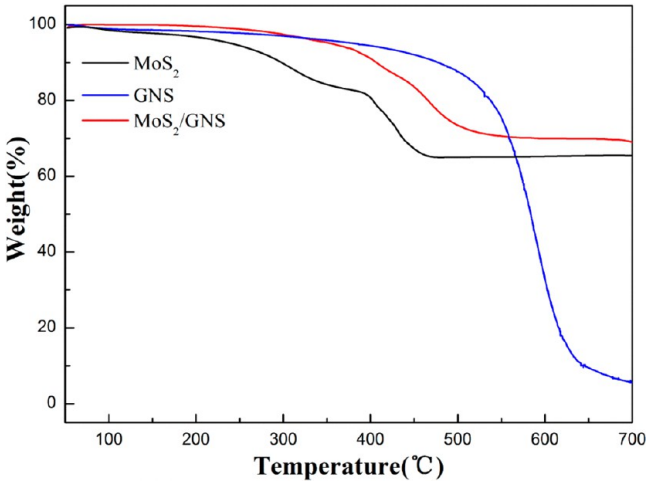

Figure 4. TG analysis curves of MoS_2, GNS, and MoS_2/GNS hybrids under air atmosphere at a heating rate of 20 °C·min^{-1}.

In comparison with pure EP, the onset degradation temperatures of MoS_2/EP,GNS/EP and MoS_2/GNS/EP composites were increased. Based on the fact that the oxidation of MoS_2 or GNS does not begin at the T_{onset} of epoxy, it is concluded that the increased T_{onset} of MoS_2/EP or GNS/EP composites is probably due to the "tortuous path" effect of MoS_2 or GNS, which restrains the osmosis of heat and the effusion of volatile decomposition products.[28] The interesting finding is that the T_{onset} of MoS_2/EP composites is higher than that of GNS/EP composites, probably on account of the high thermal conductivity of GNS which accelerates the spread of heat in the material. Furthermore, MoS_2/GNS/EP composites display the best thermostabilization with an 53 °C augment in T_{onset} compared with pure epoxy. At the T_{max} of epoxy, the oxidation of MoS_2 or GNS starts. Compared to that of pure EP, the maximum mass loss rate of MoS_2/EP composites is lower, attributed to the barrier effect of unoxidized MoS_2 and smoke suppression of molybdenum trioxide (MoO_3), that is, oxidation products of MoS_2. While GNS starts at the T_{max} of epoxy, the residues of GNS is still above 90%. So, the barrier effect of GNS is mainly responsible for the lower maximum mass loss rate of GNS/EP composites. Moreover, TG profiles (Figure 5b) show the highest char residues for MoS_2/GNS/EP composites and DTG profiles (Figure 5d) display the lowest value for MoS_2/GNS/EP composites with regard to the maximum mass loss rate, suggesting MoS_2/GNS/EP composites form the most effective barrier to hinder the quality loss during the thermal degradation process. At the stage of the decomposition of the macromolecular chains, MoS_2 on the surface of GNS is first oxidized to molybdenum oxide, and then underlying GNS begins to be oxidized. The improved thermal oxidative resistance of GNS is beneficial for the barrier effect of GNS and the generated MoO_3 has highly catalytic activity for smoke suppression, which are responsible for the lowest maximum mass loss rate of MoS_2/GNS/EP composites.

3.3. Fire Hazards Assessed by MCC. As is well-known, GNS is hoped to decrease the fire hazards of polymer materials because of its characteristic 2D carbon sheet structure. To verifying this thought, MCC was applied to describe the potential flammability performance of the epoxy composites. The heat release rate (HRR) curves of pure EP, GNS/EP, MoS_2/EP, and MoS_2/GNS/EP composites are shown in Figure 6, and the relevant data are recorded in Table 1. The incorporation of 2 wt % GNS brings about a 18.4% reduction in PHRR, compared with that of pure EP. Furthermore, the addition of MoS_2/GNS hybrids leads to the lowest PHRR value

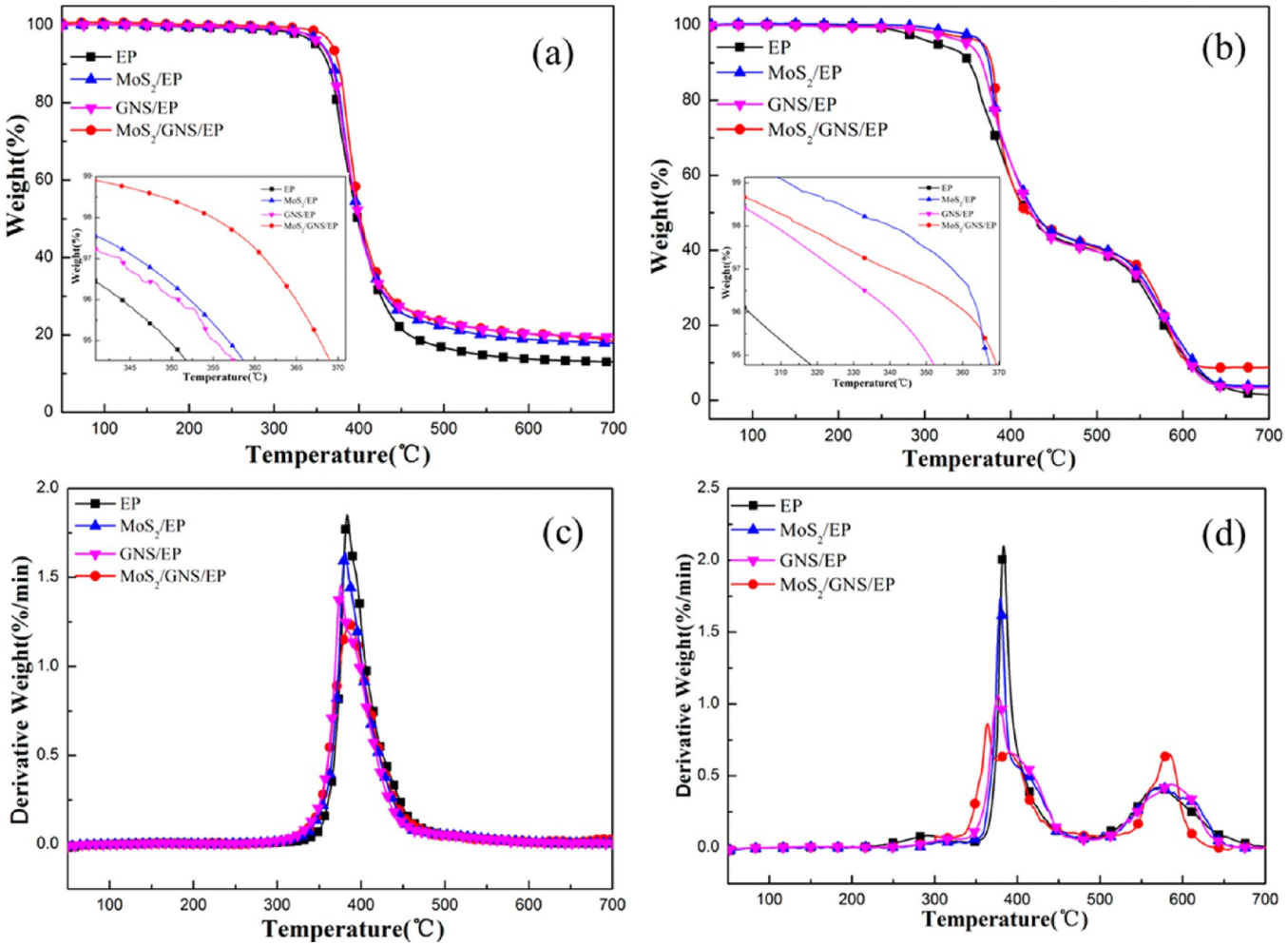

Figure 5. TG and DTG profiles for epoxy and its composites as a function of temperature under nitrogen atmosphere (a and c) and under air atmosphere (b and d).

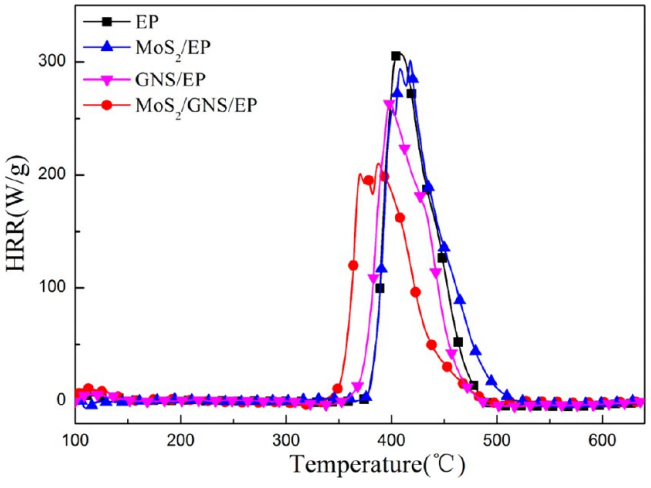

Figure 6. HRR curves of pure EP, MoS_2/EP, GNS/EP, and MoS_2/GNS/EP composites obtained from MCC.

with almost a 31.7% reduction. As well, the addition of 2 wt % MoS_2/GNS hybrids results in the lowest total heat release. The decline of PHRR and THR could be explained by thermal behaviors of pure EP and its composites in Figure 5a and c. The PHRR values of pure EP, MoS_2/EP, GNS/EP, and MoS_2/GNS/EP composites successively decrease, according with the

Table 1. MCC Data of EP, MoS_2/EP, GNS/EP, and MoS_2/GNS/EP Composites[a]

sample	PHRR ($W \cdot g^{-1}$)	THR ($kJ \cdot g^{-1}$)	T_{PHRR} (°C)
EP	309	17.1	408
MoS_2/EP	295	15.1	409
GNS/EP	261	12.6	400
MoS_2/GNS/EP	211	12.1	389

[a]PHRR: peak heat release rate. THR: total heat release. T_{PHRR}: temperature at PHRR.

successively decreased trend of their maximum mass loss rates in Figure 5c. It is generally accepted that the lower the maximum mass loss rate causes the lower the maximum release of decomposition products to burn, indicating that PHRR values would be lower. The lower THR values of GNS/EP, MoS_2/EP, and MoS_2/GNS/EP composites could be interpreted by catalytic carbonization of flame retardants. The higher char residues of GNS/EP, MoS_2/EP, and MoS_2/GNS/EP composites in Figure 5a confirm the existence of catalytic carbonization. Based on the above results and analyses, it is inferred that the mechanism of MoS_2/GNS in decreasing the flammability of EP is possibly put down to the creation of a barrier effect on the surface of the polymers, which could reduce the exchange of heat and mass between gas and condensed phases and protect the nether material from further

dx.doi.org/10.1021/ie402441g | Ind. Eng. Chem. Res. 2013, 52, 17882−17890

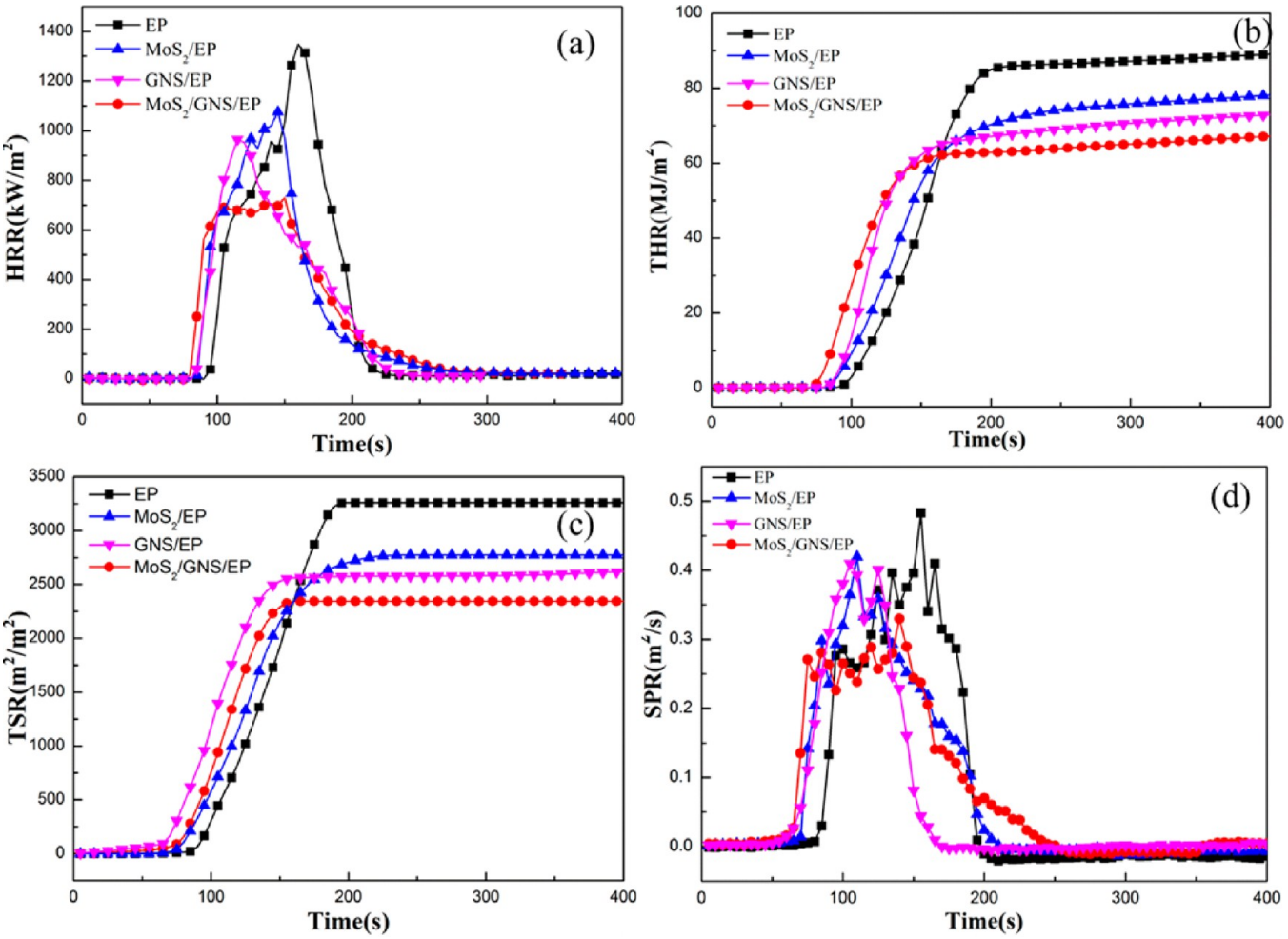

Figure 7. Heat release rate (a), Total heat release (b), total smoke release (c), and smoke production rate (d) versus time curves of epoxy and its composites obtained from cone calorimeter test.

Table 2. Cone Data of EP, MoS_2/EP, GNS/EP, and MoS_2/GNS/EP Composites[a]

sample	PHRR ($kW \cdot m^{-2}$)	THR ($MJ \cdot m^{-2}$)	TSR ($m^2 \cdot m^{-2}$)	AMLR ($g \cdot s^{-1}$)
EP	1348	87.1	3246	0.177
MoS_2/EP	1076	75.7	2734	0.149
GNS/EP	965	70.1	2486	0.128
MoS_2/GNS/EP	730	65.1	2256	0.121

[a]PHRR: peak heat release rate. THR: total heat release. TSR: total smoke release. AMLR: average mass loss rate.

combustion. However, the temperatures of PHRR for epoxy composites transfer to an earlier stage compare to pure EP, indicating the incorporation of nanofillers catalyzes the thermal degradation of epoxy, which accords with the DTG result (Figure 5c).

3.4. Fire Hazards Assessed by Cone Calorimeter. Extensive use of cone calorimeter is the most vital way to measure the flammability properties (including PHRR, THR, SPR, and TSP which are important parameters for evaluating fire hazards of materials) of numerous materials in fire conditions.[29] As shown in Figure 7a, incorporating 2 wt % GNS and MoS_2 into EP generates PHRR decrease to 965 kW/m^2 and 1076 kW/m^2, corresponding to a 28.4% and 20.2% reduction compared to that of neat EP, respectively. Furthermore, MoS_2/GNS/EP composite shows the most reduction in PHRR (approximately a 45.8% reduction) and THR (about a 25.3% reduction) in comparison with pure EP, indicating that MoS_2 and GNS have synergistic reinforcement on reducing PHRR and THR values of epoxy resins.

Figure 7c shows MoS_2, GNS, and MoS_2/GNS hybrids have an obvious influence on smoke suppression during combustion. It can be observed that the TSR value of pure epoxy resin reaches up to 3246$m^2 \cdot m^{-2}$. As expected, the incorporation of GNS into EP results to a 23.4% reduction in TSR. In the case of MoS_2/EP composites, the TSR value is also decreased to 2734 $m^2 \cdot m^{-2}$, amounting to an 15.8% reduction in contrast to neat epoxy resin. Moreover, MoS_2/GNS hybrids show the best smoke suppression on epoxy resin, up to a 30.5% reduction in TSR, probably attributed to that MoS_2 enhances barrier effect of GNS to inhibit mass loss and MoS_2 is oxidized to molybdenum oxide(MoO_3) which is an efficient smoke suppression agent. The SPR curves of EP and its composites are shown in Figure 7d. It can clearly be seen that the maximum value of SPR of MoS_2/GNS/EP is the lowest among all

dx.doi.org/10.1021/ie402441g | Ind. Eng. Chem. Res. 2013, 52, 17882−17890

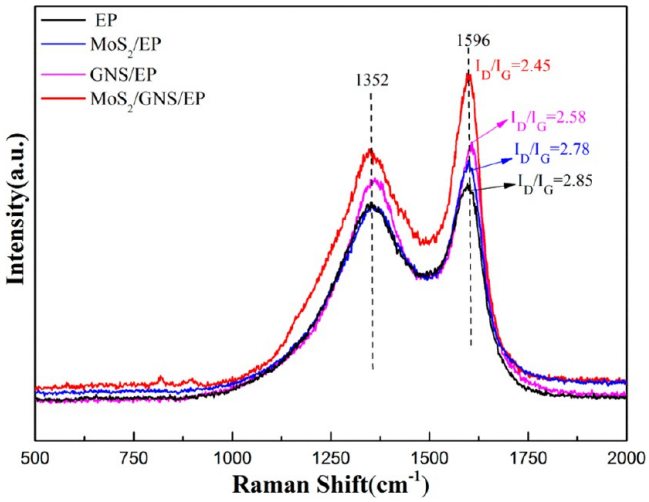

Figure 8. Raman curves of the char residues of EP and its composites after the cone calorimeter test.

composites, further proving that MoS_2/GNS hybrids perform the best smoke suppression on epoxy. With regard to the average mass rate (AMLR) recorded in Table 2, the samples having MoS_2/GNS hybrids show the lowest AMLR compared to neat EP, which conforms well to the TG, SPR, and TSR results.

3.5. Flame-Retardant Mechanism: Residual-Char Analysis. On the basis of previous reports, many different nanometer additives, such as carbon nanotubes,[30] layered double hydroxides,[31] layered silicate,[32] serve as "char enhancer" or "char swelling agent" in the condensed phase. When the condensed phase dominates the flame-retardant mechanism, the morphology, structure, and composition of the resultant char determine the efficiency of flame retardance. Hence, surveying the properties, morphology, and structure of the residual char will contribute to comprehend the work principle of flame retardants in the condensed phase.

Laser Raman spectroscopy supplies a formidable means for characterizing carbon materials. Raman spectra for the resultant char of EP, GNS/EP, MoS_2/EP, and MoS_2/GNS/EP composites after a cone calorimeter test are revealed in Figure 8. It can be distinctly seen that a D band at 1352 cm^{-1} and a G band at 1596 cm^{-1} emerge in the Raman spectra of all the samples. The former is attributed to the activation in the first order scattering process of sp^3 C atoms, while the latter is ascribed to the first-order scattering of the E_{2g} phonon of sp^2 carbons.[33] The degree of graphitization of the residual char could be computed by the ratio of accumulated intensity of the D and G bands (I_D/I_G). As is well-known, the lower the ratio of I_D/I_G, the higher graphitization degree of the resultant char.[34] The ratio of I_D/I_G for GNS/EP is lower than that of pure EP, indicating the improvement of the graphitized carbons in the residual char. Furthermore, the incorporation of the MoS_2/GNS hybrids into EP greatly decreases the ratio of I_D/I_G in comparison with that of GNS/EP, suggesting that MoS_2 tremendously enhances the function of GNS for facilitating the formation of graphitized carbons. The quality percentage of graphitized carbons of the char is related to compactness and efficiency as to thermal resistance and weight loss insulation, which offers a guardian safeguard that causes a reduce in heat and weight exchange between the fire and the polymer.

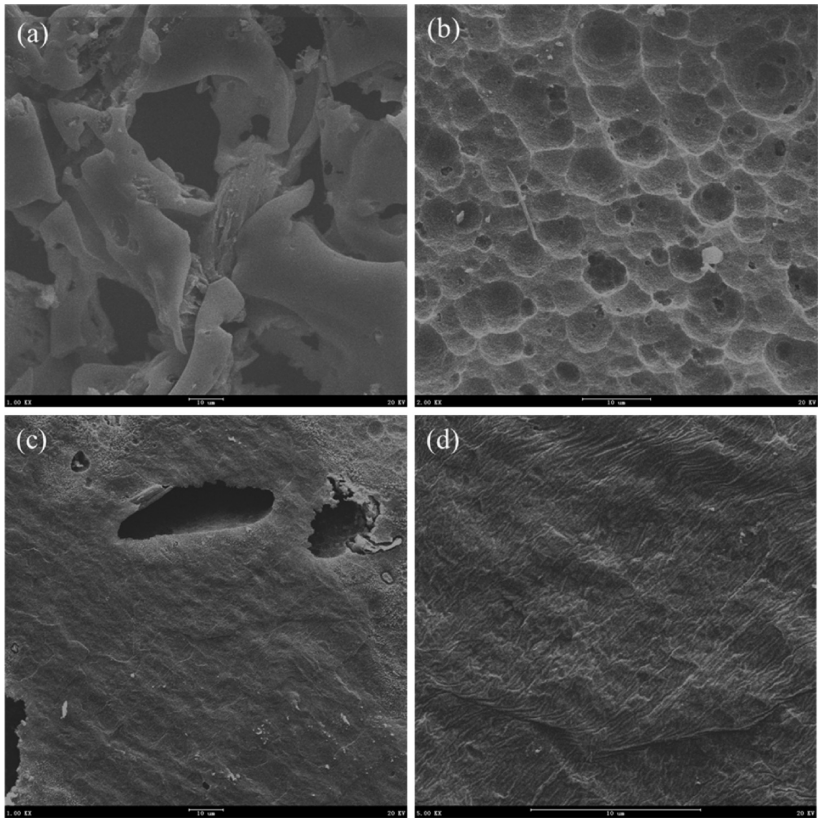

Figure 9. SEM images of the char residues after the cone calorimeter test: (a) pure EP; (b) MoS_2/EP composites; (c) GNS/EP composites; (d) MoS_2/GNS/EP composites.

dx.doi.org/10.1021/ie402441g | Ind. Eng. Chem. Res. 2013, 52, 17882−17890

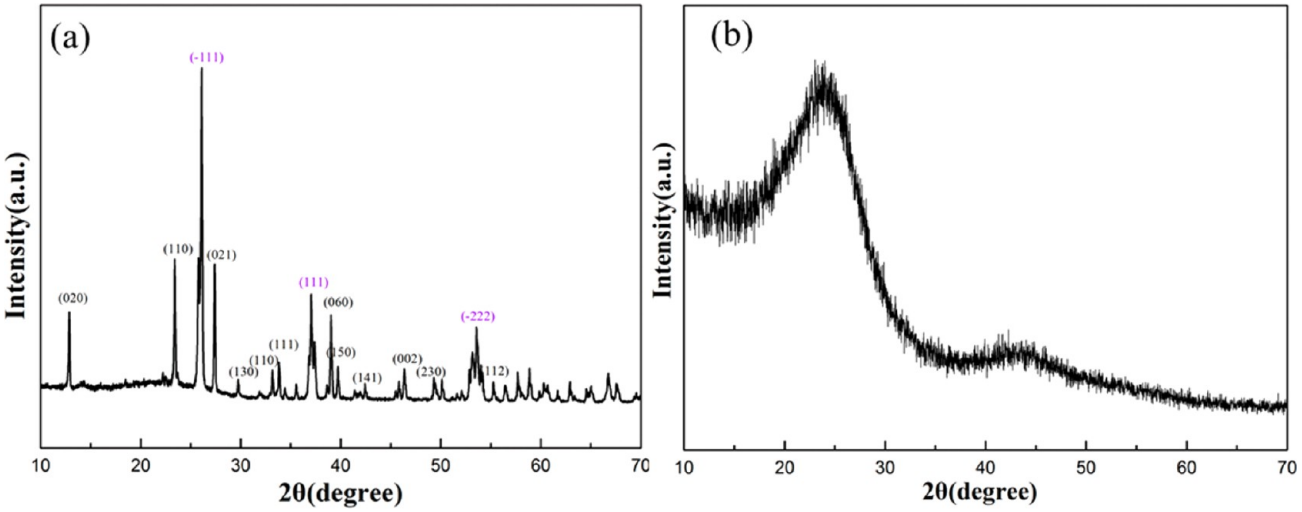

Figure 10. (a) Typical XRD patterns of exterior char: the diffraction peaks labeled in purple belong to the characteristic peaks of MoO_2, and the diffraction peaks labeled in black are assigned to the featured peaks of MoO_3. (b) Typical XRD patterns of interior char.

In order to study the relationship between flame retardant properties and morphology of the residual char, the morphologies of the residual chars gathered after the cone calorimeter test were researched by SEM. As can be observed in Figure 9a, a discontinuous char layer with many large pores appears the SEM images of pure EP. However, incorporating GNS into EP leads to a continuous and compact char layer with few pores, demonstrating GNS immensely improves the compactness of char layer. Moreover, GNS modified with MoS_2 results in a more compact char layer and no pores. The good compactness and continuity of char layer are known to be efficient and beneficial with respect to thermal and mass loss insulation.[35]

After a cone calorimeter test, hoary crystals with gloss were observed on the surface of exterior char for MoS_2/GNS/EP composites. The exterior and interior chars of MoS_2/GNS/EP composites were more surveyed by XRD analysis. As was shown in Figure.10a, the diffraction peaks labeled in black belong to the characteristic peaks of MoO_3, confirming the oxidation of MoS_2 on the surface of GNS. The typical bands at 2θ = 26.1°, 37.0°, and 53.6° are ascribed to the $(\bar{1}11)$, (111), and $(\bar{2}22)$ diffraction peaks of MoO_2, which is probably due to reduction of MoO_3 by reducing combustible gas such as hydrocarbons. Figure 10b shows two special peaks of graphite and no existence of featured diffraction peaks of molybdenum oxide, proving that molybdenum oxide can transfer and cumulate on the surface of burnable char. As a result, the presence of MoS_2 not only enhances the thermal oxidative resistance of GNS, which could effectively impede the oxygen infiltration, heat and mass transmission, and the release of combustible gases from the underlying materials during combustion, but also can be oxidized to MoO_3 that can efficiently suppress the production of smoke.[36,37]

4. CONCLUSION

In the paper, MoS_2/GNS hybrids were successfully synthesized and verified by XRD, Raman spectra, and TEM. TGA consequences display that modification of GNS with MoS_2 could improve the thermally oxidative resistance of GNS. The incorporation of 2 wt % MoS_2/GNS hybrids into epoxy resins led to a remarkable increment in T_{onset} under either air or nitrogen atmosphere, compared to that of neat epoxy. Furthermore, the PHRR, THR, and TSR values of MoS_2/GNS/EP composites were obviously decreased by 45.8%, 25.3%, and 30.5%, respectively, contrasted to those of pure epoxy, MoS_2/EP, and GNS/EP composites, which demonstrated MoS_2 and GNS had a synergistic effect on reducing fire hazards. Moreover, by the analysis of the resultant char of MoS_2/GNS/EP composite, the noteworthy improvement of the flame retardant and smoke suppression properties is primarily ascribed to two aspects: on the one hand, the addition of MoS_2/GNS hybrids result in the formation of a compact and insulating char layer to protect the inner polymer matrix from further burning; on the other hand, the formation of molybdenum oxide, a highly efficient smoke suppression agent, can decrease the production of smoke.

AUTHOR INFORMATION

Corresponding Authors

*Tel./Fax: +86-0551-63601664. E-mail: yuanhu@ustc.edu.cn.
*Tel./Fax: +86-0551-63600419. E-mail: gongxl@ustc.edu.cn.

Notes

The authors declare no competing financial interest.

ACKNOWLEDGMENTS

The work was financially supported by the National Basic Research Program of China (973 Program) (2012CB719701) and National Natural Science Foundation of China (Grant No. 11125210).

REFERENCES

(1) Geng, J. X.; Liu, L. J.; Yang, S. B.; Youn, S. C.; Kim, D. W.; Lee, J. S.; Choi, J. K.; Jung, H. T. A simple approach for preparing transparent conductive graphene films using the controlled chemical reduction of exfoliated graphene oxide in an aqueous suspension. *J. Phys. Chem. C.* **2010**, *114*, 14433−14440.

(2) Park, N. J.; Hong, S. L.; Kim, G. B.; Jhi, S. H. Computational study of hydrogen storage characteristics of covalent-bonded graphenes. *J. Am. Chem. Soc.* **2007**, *129*, 8999−9003.

(3) Yang, S. Y.; Chang, K. H.; Tien, H. Wen; Lee, Y. F.; Li, S. M.; Wang, Y. S.; M. Ma., C. C.; Hu, C. C. Design and tailoring of a hierarchical graphene−carbon nanotube architecture for supercapacitors. *J. Mater. Chem.* **2011**, *21*, 2374−2380.

(4) Kim, D. J.; Park, H. C.; Jung, J. H.; Yoon, O. J.; Park, J. S.; Yoon, M. Y.; Lee, N. E. Electrical graphene aptasensor for ultra-sensitive

detection of anthrax toxin with amplified signal transduction. *Small* **2013**, *9*, 3352−60.
(5) Syurik, J.; Ageev, O. A.; Cherednichenko, D. I.; Konoplev, B. G.; Alexeev, A. Nonlinear conductivity dependence on temperature in graphene-based polymer nanocomposite. *Carbon* **2013**, *63*, 317−323.
(6) Shi, Y. M.; Li, L. J. Chemically modified graphene: Flame retardant or fuel for combustion ? *J. Mater. Chem.* **2011**, *21*, 3277−3279.
(7) Zhang, S. P.; Song, H. Q. Preparation of β-cyclodextrin functionalized graphene and enhancement of the thermal stability. *Chem. Res. Chin. Univ.* **2012**, *33*, 1214−1219.
(8) Guo, Y. Q.; Bao, C. L.; Song, L.; Yuan, B. H.; Hu, Y. In situ polymerization of graphene, graphite oxide, and functionalized graphite oxide into epoxy resin and comparison study of on-the-flame behavior. *Ind. Eng. Chem. Res.* **2011**, *50*, 7772−7783.
(9) Wang, X.; Song, L.; Yang, H. Y.; Lu, H. D.; Hu, Y. Synergistic effect of graphene on antidripping and fire resistance of intumescent flame retardant poly(butylene succinate) composites. *Ind. Eng. Chem. Res.* **2011**, *50*, 5376−5383.
(10) Wang, X.; Hu, Y.; Song, L.; Yang, H. Y.; Yu, B.; Kandola, B.; Deli, D. Comparative study on the synergistic effect of PUSS and graphene with melamine phosphate on the flame retardance of poly(butylene succinate). *Thermochim. Acta* **2012**, *543*, 156.
(11) Kim, F.; Luo, J. Y.; Cruz-Silva, R.; Cote, L. J.; Sohn, K.; Huang, J. X. Self-propagating domino-like reactions in oxidized graphite. *Adv. Funct. Mater.* **2010**, *20*, 2867−2873.
(12) Wang, X.; Song, L.; Yang, H. Y.; Xing, W. Y.; Kandola, B.; Hua, Y. Simultaneous reduction and surface functionalization of graphene oxide with POSS for reducing fire hazards in epoxy composites. *J. Mater. Chem.* **2012**, *22*, 22037−22043.
(13) Bao, C. L.; Song, L.; Wilkie, C. A.; Yuan, B. H.; Guo, Y. Q.; Hu, Y.; Gong, X. L. Graphite oxide, graphene, and metal-loaded graphene for fire safety applications of polystyrene. *J. Mater. Chem.* **2012**, *22*, 16399−16406.
(14) Wang, X.; Zhou, S.; Xing, W. Y.; Yu, B.; Feng, X. M.; Song, L.; Hu, Y. Self-assembly of Ni−Fe layered double hydroxide/graphene hybrids for reducing fire hazard in epoxy composites. *J. Mater. Chem. A.* **2013**, *1*, 4383−4390.
(15) Chang, K.; Chen, W. X. L-Cysteine-assisted synthesis of layered MoS_2/ graphene composites with excellent electrochemical performances for lithium ion batteries. *ACS Nano* **2011**, *5*, 4720−4728.
(16) Radisavljevic, B.; Radenovic, A.; Brivio, J.; Giacometti, V.; Kis, A. Single-layer MoS_2 transistors. *Nat. Nanotechnol.* **2011**, *6*, 147−150.
(17) Li, Y.; Wang, H.; Xie, L.; Liang, Y.; Hong, G.; Dai, H. MoS_2 nanoparticles grown on graphene: An advanced catalyst for the hydrogen evolution reaction. *J. Am. Chem. Soc.* **2011**, *133*, 7296−7299.
(18) Lin, B. Z.; Ding, C.; Xu, B. H.; Chen, Z. J.; Chen, Y. L. Preparation and characterization of polythiophene/molybdenum disulfide intercalation material. *Mater. Res. Bull.* **2009**, *44*, 719−723.
(19) Zhou, K. Q.; Jiang, S. H.; Bao, C. L.; Song, L.; Wang, B. B; Tang, G.; Hu, Y.; Gui, Z. Preparation of poly(vinyl alcohol) nanocomposites with molybdenum disulfide(MoS_2): Structural characteristics and markedly enhanced properties. *RSC Adv.* **2012**, *2*, 11695−11703.
(20) Matusinovic, Z.; Shukla, R.; Manias, E.; Hogshead, C. G.; Wilkie, C. A. Polystyrene/molybdenum disulfide and poly(methyl methacrylate) /molybdenum disulfide nanocomposites with enhanced thermal stability. *Polym. Degrad. Stab.* **2012**, *97*, 2481−2486.
(21) Qian, X. D.; Song, L.; Yu, B.; Wang, B. B.; Yuan, B. H.; Shi, Y. Q.; Hu, Y. Novel organic−inorganic flame retardants containing exfoliated graphene: Preparation and their performance on the flame retardancy of epoxy resins. *J. Mater. Chem. A* **2013**, *1*, 6822−6830.
(22) Wang, X.; Song, L.; Pornwannchai, W.; Hu, Y.; Kandola, B. The effect of graphene presence in flame retarded epoxy resin matrix on the mechanical and flammability properties of glass fiber-reinforced composites. *Chem. Commun.* **2013**, *49*, 88−96.
(23) Liao, S. H.; Liu, P. L.; Hsiao, M. C.; Teng, C. C.; Wang, C. A.; Ger, M. D.; Chiang, C. L. Functionalized graphene oxide for fire safety applications of polymers: A combination of condensed phase flame retardant strategies. *Ind. Eng. Chem. Res.* **2012**, *51*, 4573−4581.
(24) Han, Y. Q.; Wu, Y.; Shen, M. X.; Huang, X. L.; Zhu, J. J.; Zhang, X. G. Preparation and properties of polystyrene nanocomposites with graphite oxide and graphene as flame retardants. *J. Mater. Sci.* **2013**, *48*, 4214−4222.
(25) Hummers, W. S., Jr.; Offeman, R. E. Preparation of graphitic oxide. *J. Am. Chem. Soc.* **1958**, *80*, 1339−1339.
(26) Frey, G. L.; Tenne, R.; Matthews, M. J.; Dresselhaus, M. S.; Dresselhaus, G. Raman and resonance Raman investigation of MoS_2 nanoparticles. *Phys. Rev. B: Condens. Matter Mater. Phys.* **1999**, *60*, 2883.
(27) Pimenta, M. A.; Dresselhaus, G.; Dresselhaus, M. S.; Cancado, L. G.; Jorio, A.; Saito, R. Studying disorder in graphite-based systems by Raman spectroscopy. *Phys. Chem. Chem. Phys.* **2007**, *9*, 1276−1290.
(28) Cao, Y. W.; Feng, J. C.; Wu, P. Y. Preparation of organically dispersible graphene nanosheet powders through a lyophilization method and their poly(lactic acid) composites. *Carbon* **2010**, *48*, 3834−3839.
(29) Cheng, K. C.; Yu, C. B.; Guo, W. J.; Wang, S. F.; Chuang, T. H.; Lin, Y. H. Thermal properties and flammability of polylactide nanocomposites with aluminum trihydrate and organoclay. *Carbohydr. Polym.* **2012**, *87*, 1119−1123.
(30) Ma, H. Y.; Tong, L. F.; Xu, Z. B.; Fang, Z. P. Functionalizing carbon nanotubes by grafting on intumescent flame retardant: Nanocomposite synthesis, morphology, rheology, and flammability. *Adv. Funct. Mater.* **2008**, *18*, 414−421.
(31) Guo, S. Z.; Zhang, C.; Peng, H. D.; Wang, W. Z.; Liu, T. X. Structural characterization, thermal and mechanical properties of polyurethane/CoAl layered double hydroxide nanocomposites prepared via in situ polymerization. *Compos. Sci. Technol.* **2011**, *71*, 791−796.
(32) Shi, Y.; Kashiwagi, T.; Walters, R. N.; Gilman, J. W.; Lyon, R. E.; Sogah, D. Y. Ethylene vinyl acetate/layered silicate nanocomposites prepared by a surfactant-free method: Enhanced flame retardant and mechanical properties. *Polymer* **2009**, *50*, 3478−3487.
(33) Fang, M.; Wang, K. G.; Lu, H. B.; Yang, Y. L.; Nutt, S. Covalent polymer functionalization of graphene nanosheets and mechanical properties of composites. *J. Mater. Chem.* **2009**, *19*, 7098−7105.
(34) Liao, S.-H.; Liu, P.-L.; Hsiao, M.-C.; Teng, C.-C.; Wang, C.-A.; Ger, M.-D.; Chiang, C.-L. One-step reduction and functionalization of graphene oxide with phosphorus-based compound to produce flame-retardant epoxy nanocomposite. *Ind. Eng. Chem. Res.* **2012**, *51*, 4573−4581.
(35) Tang, G.; Wang, X.; Xing, W. Y.; Zhang, P.; Wang, B. B.; Hong, N. N.; Yang, W.; Hu, Y.; Song, L. Thermal degradation and flame retardance of biobased polylactide composites based on aluminum hypophosphite. *Ind. Eng. Chem. Res.* **2012**, *51*, 12009−12016.
(36) Lattimer, R. P.; Kroenke, W. J. The functional role of molybdenum trioxide as a smoke retarder additive in rigid poly-(vinyl-chloride). *J. Appl. Polymer Sci.* **1981**, *26*, 1191−1210.
(37) Polka, M. The influence of flame retardant additives on fire properties of epoxy materials. *J. Civil Eng. Manage.* **2008**, *14*, 45−48.